A comprehensive evaluation of inland water quality monitoring using the long-term Landsat archive and mixture density networks

Lorena Pinheiro-Silva[1*], Xiaoxu Guo[1], Rebecca L. North[2], Greg M. Silsbe[1]

[1]Horn Point Laboratory, University of Maryland Center for Environmental Science, Cambridge, Maryland, USA.

[2]School of Natural Resources, University of Missouri-Columbia, Columbia, Missouri, USA.

[*] *Corresponding author*: lsilva@umces.edu

Keywords: Machine learning, Remote sensing, OLI, ETM+, Reservoirs, Total nitrogen, Total phosphorus.

Abstract

Nutrient enrichment of inland and coastal waters is visible from space. In these regions, chlorophyll *a* (chl-*a*), total suspended solids (TSS), and Secchi depth (Z_{SD}) constitute the most commonly targeted water quality parameters. A growing number of studies have shown that, despite not being strictly optically active, total nitrogen (TN) and total phosphorus (TP) can nonetheless be estimated from remotely sensed data with varying accuracy, underscoring that in some environments water color is a robust indicator of trophic state. This study provides a comprehensive analysis of Mixture Density Networks (MDN) model performance across a suite of water quality parameters (TN, TP, chl-*a*, Z_{SD}, and TSS) using Landsat 7–9 co-located with nearly 100 sampled reservoirs in Missouri, USA. MDN models were deployed across several pipelines that represent different combinations of atmospheric correction processors (LEDAPS/LaSRC, ACOLITE, and RAdCor), matchup windows (within ±1 and ±3 -day), feature engineering strategies (single versus multi-feature input), and model output configurations (single versus multiple-output). The median symmetric accuracy (MdSA) of model predictions was variable across parameters and pipelines. TN had the best-performing pipeline (MdSA=16.1%) and pipeline ensemble (MdSA=25.9%) followed by Z_{SD}, TSS, and TP. Chl-*a* had worst ensemble accuracy (MdSA=71.1%) and was consistently the least accurate water quality metric across pipelines. That in this dataset definitive metrics of eutrophication that include non-optically active constituents (TN and TP) can be more accurately estimated than the most widely targeted water quality parameter (chl-*a*) is discussed from theoretical and applied perspectives.

1. Introduction

Nutrient enrichment, predominantly in the form of nitrogen and phosphorus coming from agriculture runoff, municipal and industrial effluents and atmospheric deposition, is the largest anthropogenic stressor to freshwater, estuarine and coastal ecosystems (Conley et al., 2009; Smith and Schindler, 2009). As many of the symptoms of eutrophication are visible from space, satellite remote sensing of water quality is a rapidly growing field (Ogashawara et al., 2024). In a recent review examining remotely sensed metrics of trophic state (Meyer et al., 2024), chlorophyll *a* (chl-*a*), total suspended solids (TSS), and Secchi depth (Z_{SD}) constituted the most commonly targeted water quality parameters in inland and estuarine waters. Thus, satellite remote sensing has largely focused on the symptom, rather than the cause of eutrophication. This is logically a consequence of the fact that, unlike total nitrogen (TN) and total phosphorus (TP) that include colorless constituents, widely used trophic state metrics are either optically active constituents (chl-*a*, TSS) or an apparent optical property (Z_{SD}) that influences reflectance spectra.

Despite improvements in sensor technology, data accessibility, and algorithm development, chl-*a* retrievals are still largely subject to high uncertainty (Lin et al., 2018; Seegers et al., 2018). In freshwater and coastal environments, this uncertainty is often attributed to so-called Case II waters whereby the lack of covariation between chl-*a*, TSS, and chromophoric dissolved organic matter (cDOM) engenders a degree of complexity that even well-trained machine learning models struggle to overcome (Pahlevan et al., 2020). Two less noted but nonetheless important sources of uncertainty are 1) physiological processes that affect the scattering and absorption properties of a single cell (e.g., photoacclimation, pigment-packaging), and 2) changes in community composition that can result in a diversity of accessory pigments and cellular morphometry that can further decouple chl-*a* from reflectance in complex ways (Bricaud et al., 1995; Hoepffner and Sathyendranath, 1992; Sauer et al., 2012). Indeed, it is worth noting that chl-*a* retrievals of NASA's default OCI algorithm from the latest MODIS Aqua reprocessing version (R2022.0.1) that are predominantly Case-I waters, have a mean absolute error (MAE) of 1.69. While a global ocean dataset undoubtably encapsulates greater taxonomic and physiological diversity than targeted inland and coastal ecosystems, high uncertainty in chl-*a* retrievals from remote sensing reflectance remains an open challenge.

Given the undisputed utility of synoptic water quality metrics from space alongside the inherent large uncertainty accuracy of chl-*a* retrievals, a growing number of studies have shown that non-optically active parameters including TP and TN can be indirectly detected by satellite sensors, despite lacking spectral signatures, due to their strong correlation with optically active constituents (Xiong et al., 2022). Several methods have been developed to estimate nutrient concentrations from satellite imagery, including empirical band ratio algorithms based on statistical relationships (Dong et al., 2020; Li et al., 2017; Sun et al., 2014; Wu et al., 2010) and machine learning (ML) models (Chebud et al., 2012; Guo et al., 2024, 2022, 2021; Xiong et al., 2022; Zhu et al., 2024, 2022). Among these methods, ML improves the ability to capture complex relationships among optically active constituents (OACs), non-OACs, and remote sensing reflectance data (R_{rs}), and therefore, has strong potential to enable the direct retrieval of non-OACs from R_{rs} (Xiong et al., 2022). In this context, probabilistic neural network (NN) models have emerged as a promising alternative as they can improve retrieval accuracy by modeling the output as a probability distribution, estimating a range of likely values rather than a single prediction (i.e., point-based modeling), while also quantifying prediction uncertainty (Saranathan et al., 2024). Among probabilistic NN models, Mixture Density Network (MDN) has been applied to inland and coastal waters on a global scale (Pahlevan et al., 2022, 2021b, 2020; Smith et al., 2021) and shown to outperform several commonly used methods for retrieving water quality parameters (Pahlevan et al., 2020; Smith et al., 2021). However, to date, these approaches have not been tested for TP and TN retrieval, particularly in optically complex inland waters.

This study aims to evaluate the feasibility of applying MDN models to atmospherically corrected Landsat imagery from the Enhanced Thematic Mapper Plus (ETM+) and Operational Land Imagers (OLIs) aboard Landsat-7, Landsat-8, and Landsat-9 to retrieve TN and TP, as well as commonly retrieved water quality parameters, including chl-*a*, Z_{SD}, and TSS. MDN models were developed using paired *in situ* measurements from 83 waterbodies in Missouri, USA. First, we evaluated two feature engineering strategies: one using only the original spectral bands and another combining single spectral bands with spectral band ratios and indices. The best-performing feature engineering strategy was then used to evaluate the capability of MDN models to simultaneously estimate multiple water quality parameters, allowing assessment of whether including co-varying constituents improves retrieval performance (Pahlevan et al., 2022; Smith et al., 2021). We also evaluated the impact of different atmospheric correction (AC) processors (LEDAPS/LaSRC, ACOLITE, and ACOLITE-RAdCor) and time windows from the satellite overpass (±1-day and ±3-day) on algorithm performance. By developing a comprehensive framework for combining satellite remote sensing with explainable machine learning, our findings provide guidance for future applications of remote sensing to inland water quality monitoring.

2. Materials & Methods

2.1 Study site and water quality data sources

Missouri, located in the central United States (Figure 1), spans six Environmental Protection Agency (EPA) ecoregions and exhibits a strong south-to-north nutrient gradient that reflects regional land-use patterns. Reservoirs in the plains of northern and western Missouri are largely surrounded by cropland agriculture and are generally more eutrophic than those in the forested Ozark Highlands located in the south (Jones et al., 2008b). A recent study showed that most Missouri reservoirs are green, with dominant wavelengths between 538–555 nm, closer to the brown than the blue color endmember (Pinheiro-Silva et al., 2025). Overall, Missouri reservoirs span wide ranges of surface area (0.003 – 335,50 km^2), morphometry, and watershed characteristics (Jones et al., 2008a), encompassing broad environmental gradients in trophic status and land cover across the state.

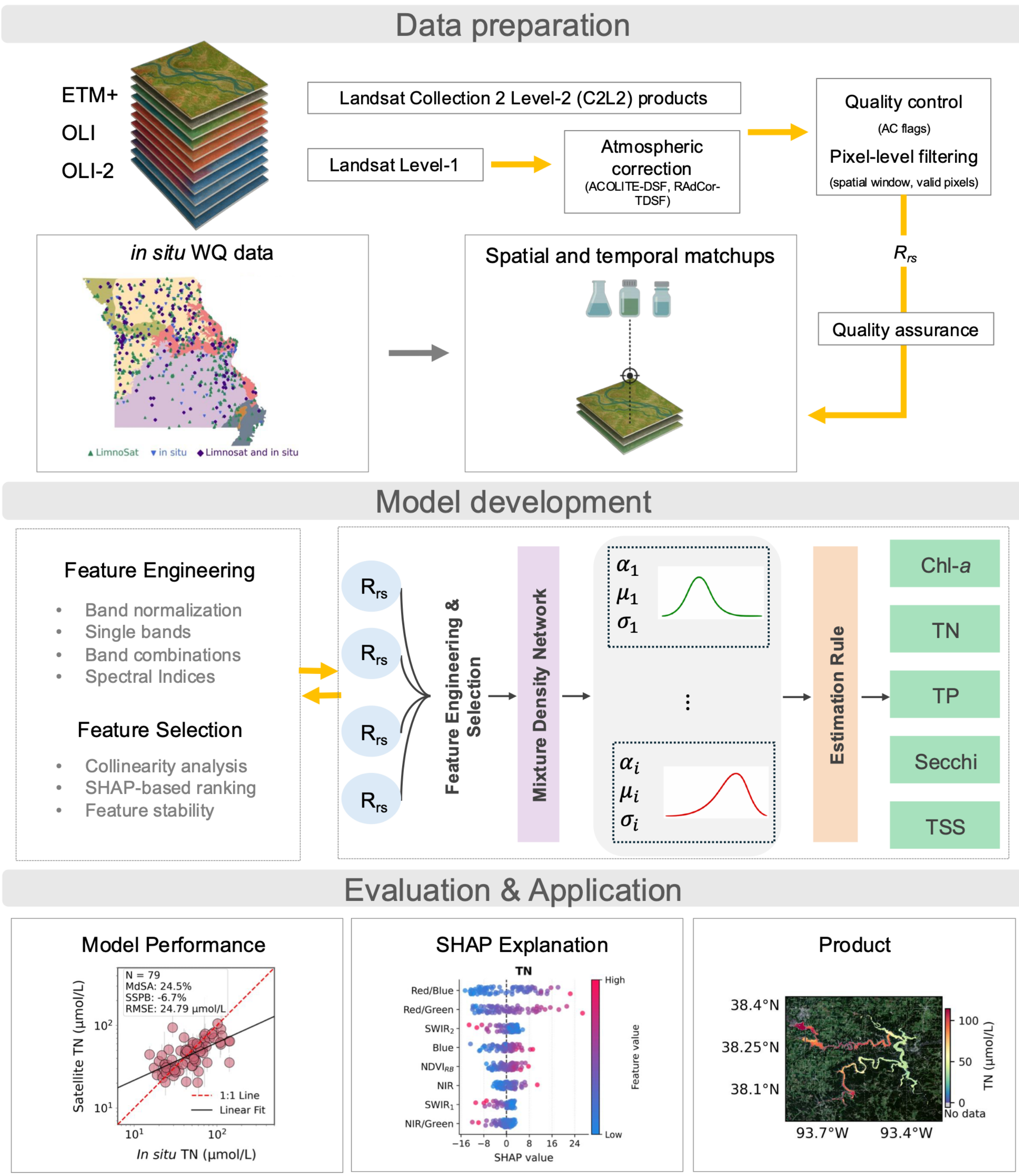

Figure 1: Flowchart illustrating data preparation, model development and model evaluation and application.

Long-term water quality records (1999 – 2023) from 83 waterbodies in Missouri (Supplementary Table 1) were obtained from the Statewide Lake Assessment Program (SLAP) and the community science led Lakes of Missouri Volunteer Program (LMVP). Measurements of chl-*a*, Z_{SD}, TN, TP, and TSS were collected across multiple reservoirs, based on surface or integrated epilimnetic samples taken three to four times between May and October near the deepest (i.e., near-dam) sites in each reservoir (Jones et al., 2024a, 2024b; North et al., 2025). Water transparency (Z_{SD}) was measured using a Secchi disk. Water samples were collected and stored in high density polyethylene (HDPE) bottles, then processed and frozen until analysis for uncorrected chlorophyll *a* (chl-*a*; µg/L), total nitrogen (TN; µmol/L), total phosphorus (TP; µmol/L), and suspended solids (TSS; mg/L) following standard methods (Supplementary Table 2). Sampling and analytical procedures were consistent throughout the study period for TSS but varied for chl *a*, TP, and TN. In total, the *in situ* dataset comprised 13,855 observations after quality control procedures. Quality control included removal of measurements flagged as below detection limits or failing laboratory replicate criteria. Summary statistics for all water quality parameters are presented in Table 1.

Table 1. Descriptive statistics summary of *in situ* water quality parameters collected in Missouri reservoirs during the study period. Std refers to standard deviation, Chl-*a* to chlorophyll-*a*, TN to total nitrogen, TP to total phosphorus, Z_{SD} to Secchi disk depth, and TSS to total suspended solids. n is the number of samples.

Parameter (unit)	Chl-*a* (µg/L)	TN (µmol/L)	TP (µmol/L)	Z_{SD} (m)	TSS (mg/L)
n	13,722	13,684	13,687	13,582	13,135
Mean	24.87	55.97	1.67	1.34	8.2
Std	30.09	34.56	1.80	1.02	9.5
Min	0.10	1.43	0.02	0.01	0.2
Median	15.00	48.54	1.13	1.02	6.1
Max	641.70	530.34	24.77	8.61	494.0

2.2 Atmospheric correction (AC) approaches

Level-1 Terrain Precision (L1TP) data from Enhanced Thematic Mapper Plus (ETM+), Operational Land Imager (OLI), and Operational Land Imager-2 (OLI-2) sensors onboard

Landsat 7, 8, and 9, respectively were downloaded from the USGS EarthExplorer portal for the period 1999 to 2023. These were then passed through two different AC pipelines detailed below and are compared against USGS Collection 2 Level-2 surface reflectance products that were also downloaded for each Level-1 scene.

Level-1 imagery was atmospherically corrected to retrieve water-leaving remote sensing reflectance (R_{rs}; sr^{-1}) using the free and open source ACOLITE (Atmospheric Correction for OLI 'Lite' software version 20250402.0, Vanhellemont, 2019; Vanhellemont and Ruddick, 2018). Atmospheric correction was conducted using the Dark Spectrum Fitting (DSF) algorithm optimized for turbid waters, which has consistently demonstrated superior performance compared with alternative processors, particularly in inland and coastal turbid waters (Maciel and Pedocchi, 2022; Pahlevan et al., 2021a; Renosh et al., 2020; Wang et al., 2019). We employed a fixed aerosol optical thickness (AOT) estimation for the DSF algorithm, which provides more stable results for small reservoirs compared to the tiled approach. To maximize the number of valid matchups, the Short-Wave Infrared (SWIR) threshold was increased to 0.05 to avoid misidentifying highly turbid water as land, and the cirrus cloud threshold was relaxed to 0.025 to minimize the exclusion of valid observation under thin atmospheric haze. Furthermore, the optional residual glint correction using the SWIR bands was not applied, and pixels with negative reflectance in specific bands were retained to prevent the loss of data in highly absorbing waters. To ensure spatial consistency, input tiles were merged when necessary, and a bounding box with 5 km buffer was applied around each reservoir's sampling point.

To address adjacency effects, which are particularly relevant for small and narrow inland waterbodies, we compared standard ACOLITE processing with an alternative workflow that included the Remote Sensing Adjacency Correction (RAdCor) module, recently implemented in

ACOLITE (Castagna and Vanhellemont, 2025). This module implements a Topographic-adjacency corrected DSF (TDSF), a physics-based method that uses a radiative transfer-derived (6SV) atmospheric diffuse Point Spread Function (PSF) to specifically correct for radiance scattered from surrounding land pixels. The RAdCor workflow was customized in the same way as the ACOLITE, with the addition of the adjacency correction module.

2.3 Spatiotemporal data matchup

To create satellite matchup datasets, atmospherically corrected scenes (LEDAPS/LaSRC, ACOLITE, and RAdCor) were paired with *in situ* measurements within a ±1 and ±3 day time window of the satellite overpasses (Figure1). A 3x3 pixel window was centered on a "safest pixel" identified through a custom automated Python workflow designed to minimize land-adjacency effects while remaining close to the near-dam sampling location. This "safest pixel" was defined as the pixel within the valid water mask with the maximum Euclidean distance to the nearest shoreline, identified using a dynamic search radius centered on the *in situ* station coordinates. To account for diversity of reservoir sizes, the search radius was set to 30 m for reservoirs <0.1 km^2, 60 m for reservoirs 0.1km^2, and 90 m for reservoirs > 1 km^2.

Data quality was further ensured by applying a continuity filter, requiring a 95% valid-pixel density within a 7x7 neighborhood (210 x 210 m) around the centered pixel. For ACOLITE products (DSF and TDSF-RAdCor), pixels were excluded based on internal quality flags. For the LEDAPS/LaSRC Level-2 products, the QA_PIXEL band was used to exclude pixels contaminated by clouds, shadows, or aerosols. Any matchup was discarded if five or more pixels were flagged as invalid (six or more pixels for Landsat 7). The final reflectance values were calculated as the median of the valid pixels within the 3x3 pixel window. Level-2 Surface

Reflectance (SR) values were radiometrically scaled and converted to remote sensing reflectance (R_{rs}; sr^{-1}) by dividing by π ($R_{rs} = SR/\pi$). Any reflectance containing negative values ($R_{rs} < 0$) or unrealistic high values ($R_{rs} > 0.2$) were excluded. The final datasets consist of LEDAPS/LaSRC, ACOLITE, and RAdCor R_{rs} values paired with near-concurrent (±1 and ±3 day) *in situ* measurements of chl-*a*, TN, TP, Z_{SD}, and TSS across multiple reservoirs. The final datasets contain samples from different water types, as evidenced by the broad WQ distribution (Figure 2). To ensure the quality of the matchup datasets, a preprocessing workflow was implemented consisting of outlier removal and data transformation.

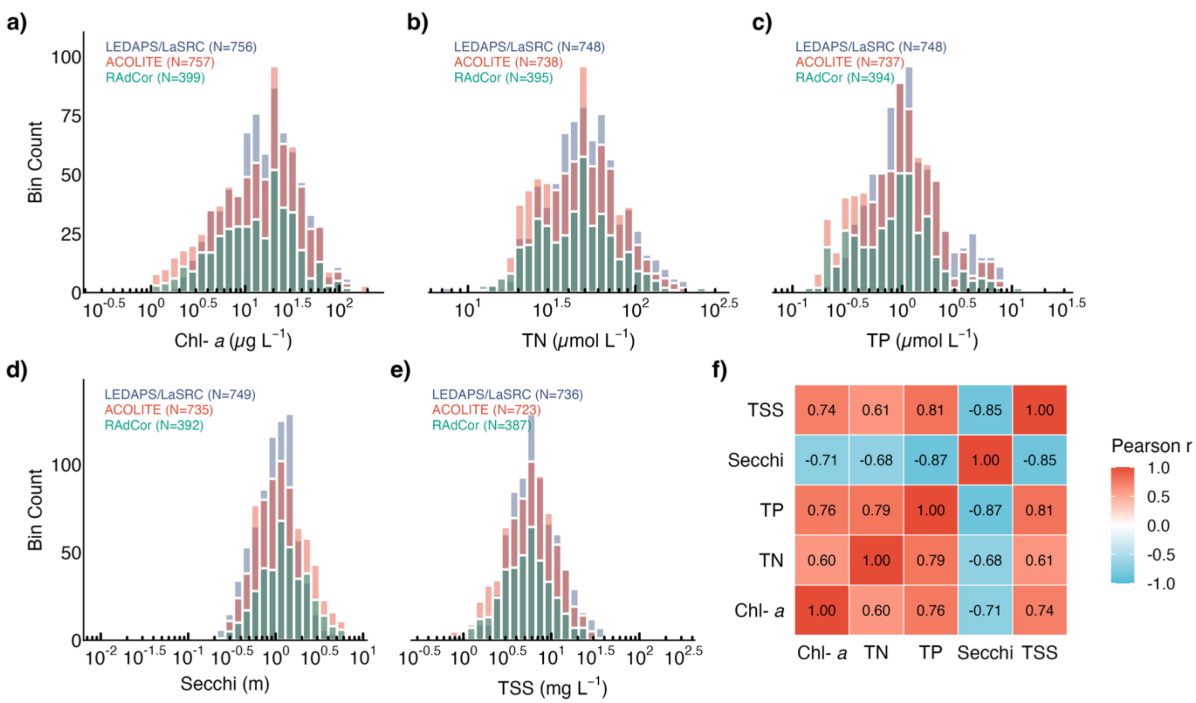

Figure 2: Frequency distribution of water quality parameters for which R_{rs} spectra were available using ±3-day (a–e) matchup window from the satellite overpasses. Histograms represent matchups for three atmospheric correction methods: LEDAPS/LaSRC, ACOLITE and RAdCor. Panels represent: (**a**) chlorophyll *a*; (**b**) total nitrogen; (**c**) total phosphorus; (**d**) Secchi disk depth; and (**e**) total suspended solids. Sample sizes (N) for each method are indicated within the panels. Panel (**f**) shows the Pearson correlation among the log10-transformed water quality variables from the RAdCor dataset.

2.4 Mixture Density Network

To estimate water quality (WQ) parameters from R_{rs}, we employed mixture density networks (MDNs; Bishop, 1994), a class of neural networks that model the conditional probability distribution of target variables given a set of input features, allowing uncertainty and potentially multimodal input-output relationships to be represented. MDNs model the conditional probability distribution as a mixture of multiple Gaussian functions, parameterized by their means, standard deviations, and mixing coefficients. The model structure consists of one input layer, one or more hidden layers, and one output layer (Figure 1). In this study, the MDN model was implemented using a modified version of the Python-based MDN library (Smith et al., 2021), adapted for the training and evaluation workflow used here.

In order to improve generalization, WQ variables were log-transformed. The feature data (R_{rs}) were then processed using a RobustScaler to reduce the influence of potential outliers by centering the data based on the interquartile range (IQR), followed by a MinMaxScaler to scale the features to the range -1 to 1. This normalization strategy reduces differences in numerical magnitude among input features and facilitates model training. The data were split at a ratio of 80:20 for model training and independent testing, respectively. The model architecture, selected based on inspection of training and validation loss curves, was defined with a depth of three hidden layers (*n_layers* = 3) with 32 neurons each (*n_hidden* = 32). To capture complex, non-linear bio-optical relationships, we employed the Rectified Linear Unit activation function (activation = 'relu'). The probabilistic output was parameterized using five Gaussian mixtures (*n_mix* = 5). Bagging was enabled (*use_bagging* = 1) and 20 model rounds were performed (*n_rounds* = 20). Other key parameters were set as follows: $l2 = 10^{-4}$, $lr = 10^{-4}$, and *n_iter* = 10,000, while other parameters were kept at their default values.

Retrieval models for chl *a*, TN, TP, Z_{SD}, and TSS were developed both individually (single-parameter retrieval) and jointly (multiple-parameter retrieval) to evaluate whether jointly predicting WQ parameters improved retrieval performance (Smith et al., 2021). ML models are particularly well suited for simultaneous retrieval, as they account for correlations and inter-dependencies among multiple targets, helping them learn shared patterns and potentially improving predictive performance (Saranathan et al., 2024). In total, we ran 26 model combinations using chl *a*, TN, TP, Z_{SD}, and TSS for each AC processor (LEDAPS/LaSRC, ACOLITE, and RAdCor) and matchup window combination (±1 and ±3 day). To evaluate whether jointly predicting WQ parameters improved retrieval performance relative to single-parameter retrieval, we used the non-parametric Mann-Whitney U test.

2.5 Feature engineering and selection

Feature engineering involved the evaluation of two feature strategies. The first used only the original spectral bands (Blue, Green, Red, NIR, SWIR1, and SWIR2). The second strategy combined the single spectral bands with additional engineered predictors, including band ratios and indices derived from those bands (Supplementary Table 3). To mitigate multicollinearity, an initial feature selection was performed by calculating Spearman's correlation coefficients among all inputs; highly redundant features were excluded using a threshold of $|r| > 0.85$. Note that this was performed for each pipeline (i.e., AC processor and time window combination), so not all features were consistent across pipelines (Supplementary Figures 1–5). Feature importance was quantified using the Shapley Additive exPlanations (SHAP) framework (Figure 1), which quantifies the contribution of each feature to a model prediction relative to a baseline prediction. Based on cooperative game theory (Shapley, 1953), SHAP values capture both the magnitude and direction (positive or negative) of a feature's influence (Zhu et al., 2024). The absolute SHAP value represents the magnitude of a feature's contribution, while positive and negative SHAP values indicate whether the feature value increases or decreases the model's prediction relative to the baseline. Finally, global feature importance was calculated as the mean of the absolute SHAP values across all observations.

2.6 Predictive performance

To evaluate the performance of MDN models, we used the Median Symmetric Accuracy (MdSA) and Signed Symmetric Percentage Bias (SSPB; Morley et al., 2018). For retrieval evaluation, point estimates were derived from the man of the Gaussian component with the highest mixture probability, and predictions were aggregated across 20 model rounds using the median. Median, rather than mean statistics were adopted as they are more robust to outliers (Seegers et al., 2018). MdSA is a measure of predictive accuracy, whereas SSPB describes the systematic direction of error, indicating whether predictions are over- or under- estimated on average. The performance metrics were calculated according to Morley et al. (2018) as follows:

$$MdSA\ (\%) = 100\left[exp\left(median\left(\left|\ln\frac{P_i}{O_i}\right|\right)\right) - 1\right] \tag{1}$$

$$SSPB\ (\%) = 100 * sign(M) * e^{|M|-1},\ M = median\left(\ln\left(\frac{P_i}{O_i}\right)\right) \tag{2}$$

where *P* and *O* represent the predicted and observed value, respectively. These metrics provide a more robust and symmetric assessment of model performance and are appropriate given the approximately log-normal distribution of WQ data (Figure 2), and because uncertainty is likely to increase with observed values (Seegers et al. 2018). For example, predicted and observed values of 4 and 2 yield an MdSA of 100% and a SSPB of 200%, and predicted and observed values of 1 and 2 also yield an MdSA of 100% and an SSPB of -200%; thus, each prediction differs from the observed value by 100% with two-fold bias. In addition to the above metrics, we also calculated Root Mean Square Error (RMSE) in linear space (original units) and median absolute error (MdAE) in log space (Seegers et al., 2018), as well as slopes and R^2 values from linear regression fits, to allow comparisons with previous studies.

Results

Performance assessment of single-output retrievals

Performance metrics were variable across parameters and the twelve pipelines (3 AC processors x 2 matchup windows x 2 feature engineering input, Supplementary Tables 4–8). To evaluate how the different pipelines impacted model performance, we first averaged MdSA and SSPB across the five WQ parameters for individual pipelines (Table 2). As a second metric of pipeline performance, a ranking system is shown (1 = most accurate; 12 = least accurate) that represents the average ranking of individual WQ parameter across 12 pipelines (Table 2). The highest ranked pipeline (mean rank = 2.2) employed the RAdCor AC processor, a ±3-day matchup window, and feature engineering that included band combinations (Figure 3). The second highest ranked pipeline (mean rank = 4.2) employed the ACOLITE AC processor with a ±1-day matchup window and feature engineering that included band combinations.

Table 2: Model performance metrics averaged across all five water quality parameters for each combination of multi- versus single- band feature engineering, ±1- versus ±3-day time windows, and three different atmospheric correction (AC) processors. **n** is the sum of testing data sample sizes across the five water quality parameters.

Feature engineering	**Time window**	**AC processor**	**n**	**Mean Model Ensembles**		
				MdSA	**SSPB**	**Rank**
Multi-feature	±1-day	LEDAPS/LaSRC	345	47.0%	-12.8%	8.4
		ACOLITE	338	37.7%	-8.6%	4.2
		RAdCor	189	43.0%	-8.6%	7.6
	±3-day	LEDAPS/LaSRC	750	37.4%	-8.6%	4.6
		ACOLITE	740	39.8%	2.2%	5.2
		RAdCor	395	34.7%	1.4%	2.2
Bands-only	±1-day	LEDAPS/LaSRC	345	44.8%	-10.8%	7.4
		ACOLITE	338	52.9%	-17.2%	11.0
		RAdCor	189	44.5%	-6.4%	7.8
	±3-day	LEDAPS/LaSRC	750	37.8%	-3.6%	4.8
		ACOLITE	740	43.6%	1.0%	6.4
		RAdCor	395	39.9%	-2.9%	5.8

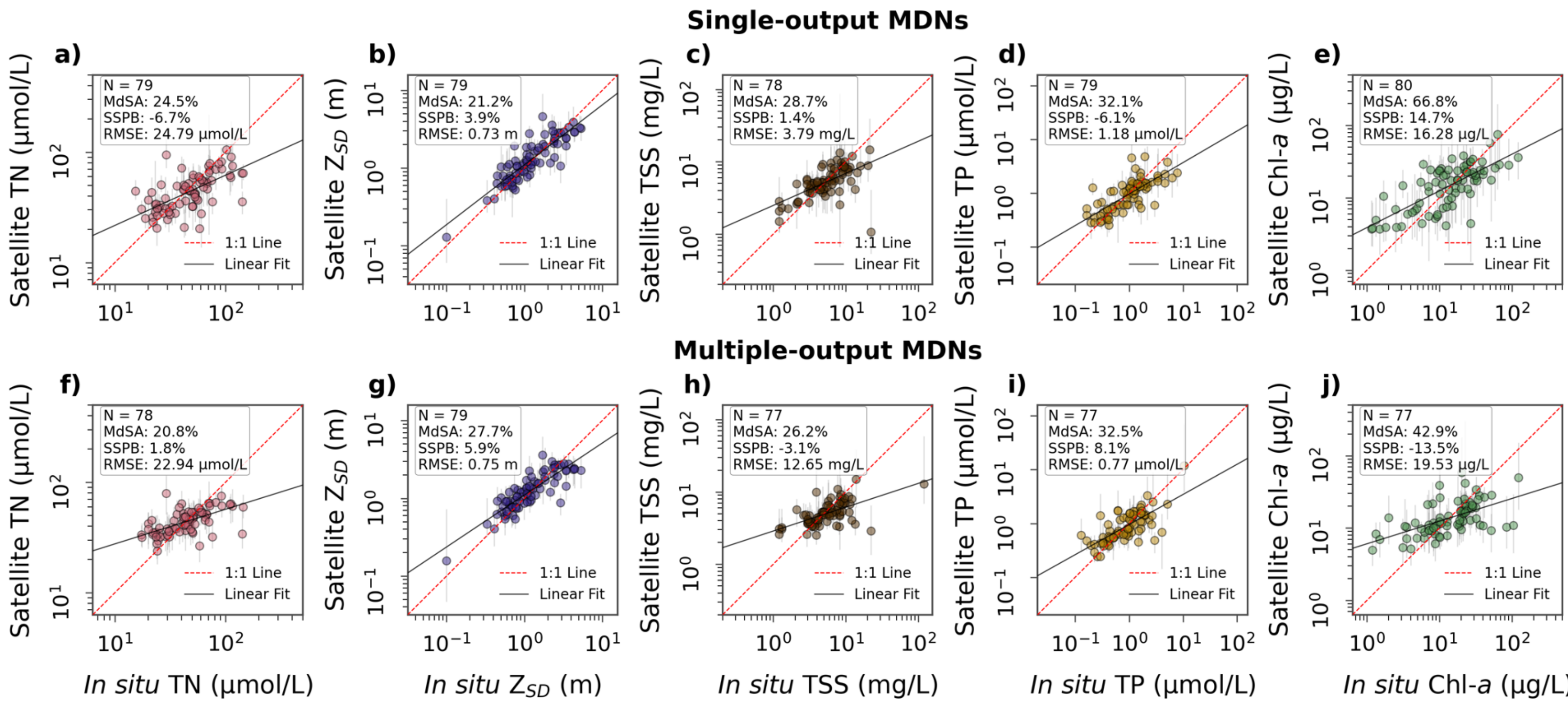

Figure 3: Performance of the MDN single-output models (a–e) and multiple-output models (f–j) using RAdCor atmospherically corrected imagery, ±3-day matchup window, and the multi-feature engineering strategy. Model performance was evaluated using the log-transformed metrics, median symmetric accuracy (MdSA) and signed symmetric percentage bias (SSPB), as well as the root mean square error (RMSE) in linear space, expressed in the units of each parameter. The red dotted line denotes the 1:1 relationship, and the gray solid line denotes the fitted linear regression. The number of samples (N) is shown in each panel. Panels (**a, f**) correspond to total nitrogen (TN; µmol/L); (**b, g**) Secchi disk depth (Z_{SD}; m); (**c, h**) total suspended solids (TSS; mg/L); (**d, i**) total phosphorus (TP; µmol/L); and (**e, j**) chlorophyll-a (chl-*a*; µg/L).

To further explore how pipeline components impacted model predictions, performance metrics were averaged across shared architecture. Beginning with feature engineering, MDN models that included band combinations have on average improved accuracy and lower bias (MdSA = 39.9%, SSPB = -5.8%) than models with only six single Landsat bands feature inputs (MdSA = 43.9%, SSPB = -6.7%). Overall, the best-performing pipeline for each WQ parameter were those that employed band combinations rather than single bands (Table 3). Across AC processors, RAdCor, on average, slightly outperformed (MdSA = 40.5%, SSPB = -4.1%) LEDAPS/LaSRC (MdSA = 41.7%, SSPB = -8.9%), which slightly outperformed ACOLITE (MdSA = 43.5%, SSPB = -5.7%). Pipelines that used ±3-day matchup window more than doubled the number of matchups (Table 2), and on average have improved accuracy and lower bias (MdSA = 38.8%, SSPB = -1.7%) compared to the more data poor ±1-day matchup window (MdSA = 45.0%, SSPB = -10.7%). That said, the best performing pipelines for TN and TP both used ±1-day pipelines (Table 3).

Table 3: Model performance metrics for individual water quality parameters averaged across an ensemble of pipelines (3 AC processors x 2 time windows, multi-feature input, single parameter output). The best performing pipeline for each parameter is also shown. The fractional **n_{ens}** is the average n across the 6 pipelines, n is testing data sample size for the given pipeline. AC refers to atmospheric correction.

	Mean Pipeline Ensemble				Best Performing Pipeline			
Parameter	**n_{ens}**	**MdSA**	**SSPB**	**Rank**	**Pipeline**	**n**	**MdSA**	**SSPB**
TN	92	25.9%	-4.6%	1.5	±1-day RAdCor	38	16.1%	-5.0%
Z_{SD}	92	30.4%	4.0%	2.0	±3-day RAdCor	79	21.2%	4.0%
TSS	91	34.6%	-7.8%	3.2	±3-day RAdCor	75	28.7%	1.0%
TP	92	37.6%	-9.0%	3.3	±1-day ACOLITE	67	29.1%	-16.0%
Chl-*a*	94	71.1%	-11.6%	5.0	±3-day LEDAPS/LaSRC	152	58.3%	-12.0%

Table 3 shows the performance metrics for individual WQ parameters averaged across all pipelines that employ band combinations as feature inputs, as well as the best performing pipeline for each WQ parameter. As above, WQ parameters were ranked within each pipeline (1 = most accurate, 5 = least accurate), and these ranks were averaged across pipelines. TN achieved the highest accuracy and second lowest absolute bias (MdSA = 25.9%, SSPB = -4.6%) across the pipelines. Across individual pipelines, TN had either the highest or second highest retrieval accuracy across the five WQ parameters. The best performing pipeline for TN (MdSA = 16.1%, SSPB = -5.0%) was RAdCor with a ±1-day matchup window and feature engineering that included band combinations. Averaged across pipelines, Z_{SD} and TSS had the second and third best accuracy (MdSA = 30.4% and 34.6% respectively), and the top performing pipeline for both parameters (MdSA < 30%) was RAdCor with a ±3-day matchup window and feature engineering that included band combinations. Averaged across pipelines, TP has a moderate accuracy (MdSA = 37.6%) and a notable negative bias (SSPB = -9%). The best performing pipeline for TP (MdSA = 29.1%, SSPB = -16.0%) employed ACOLITE with a ±1-day matchup window and feature engineering that included band combinations. Finally, chl-*a* averaged across pipelines had the lowest accuracy (MdSA = 71.1%) and was consistently the least accurate WQ parameter across pipelines. The top performing pipeline for chl-*a* (MdSA = 58.3%, SSPB = -12.0%) was LEDAPS/LaSRC with a ±3-day matchup window.

Single- vs. multiple-output retrievals

Simultaneous WQ retrievals were performed for every permutation for each of the five WQ variables (n = 15) across 6 pipelines (3 AC processors x 2 matchup windows, multi-feature engineering only). To facilitate a comparison to Table 3, error metrics for each parameter were averaged across pipelines, and the best performing pipeline was identified (Table 4). Based strictly on the ensemble means (n = 90), single-output models outperformed multiple-output models across all five WQ parameters. At this ensemble level, increasing the number of simultaneously retrieved WQ parameters generally degraded model accuracy across parameters (Supplementary Table 9). The mean MdSA of models returning two predictors (MdSA = 41.9%) was lower for models that returned three (MdSA = 43.6%), four (MdSA = 46.0%) and all five (MdSA = 48.6%) WQ parameters. However, the best performing pipelines with multiple-outputs configuration yielded more accurate WQ retrievals than the equivalent single-output model for every parameter except TN (Table 4). Four of these best-performing pipelines employed RAdCor atmospheric correction.

Table 4: Model performance metrics for individual water quality parameters averaged across an ensemble of pipelines (3 AC processors x 2 time windows, multi-feature input, multiple parameter output). The best performing pipeline for each parameter is also shown. The fractional **n_{ens}** is the average n across the 6 pipelines, n is testing data sample size for the given pipeline. AC refers to atmospheric correction.

Parameter	**Mean Pipeline Ensemble**			**Best Performing Model**				
	n_{ens}	**MdSA**	**SSPB**	**Pipeline**	**Predicted**	**n**	**MdSA**	**SSPB**
TN	90	30.8%	-2.2%	±1-day RAdCor	TN, chl-*a*	38	19.2%	2.1%
Z_{SD}	90	32.6%	0.0%	±1-day LEDAPS/LaSRC	TN, Z_{SD}, TSS	67	19.6%	-2.9%
TSS	90	38.7%	-0.3%	±3-day RAdCor	TN, TP, chl-*a*, TSS	77	26.2%	-3.1%
TP	90	42.8%	-0.0%	±1-day RAdCor	TP, chl-*a*	38	28.7%	-3.2%
Chl-*a*	90	75.8%	-1.4%	±3-day RAdCor	TN, TP, chl-*a*, TSS	77	42.9%	-13.5%

The performance of each multiple-output permutation for a given parameter is shown graphically for the best performing pipeline (RAdCor processor, ±3-day matchup window) where each circle represents one permutation color coded by MdSA rank across permutations (Figure 4). Despite the ensemble showing degraded accuracy with increasing parameters, the combination of chl-*a*, TN, TP, and TSS yielded the most accurate estimates of chl-*a* and TSS across this and all other pipelines (Table 3). However the same MDN model showed marginally reduced performance in TP and TN (Figure 4, Supplementary Table 9). TN had the best accuracy when retrieved alongside chl-*a* and Z_{SD}, while the single output models of Z_{SD} and TP had better accuracy than any multiple-output model shown in Figure 4. To better assess whether or not the inclusion of a specific WQ parameter impacted the retrieval of a second parameter, the distributions of parameter-specific MdSA values with and without a second parameter were compared non-parametrically (Mann-Whitney, $p<0.05$). For the RAdCor ±3-day matchup window pipeline, the inclusion of TSS led to statistically more accurate retrievals of chl-*a* and TP, while the inclusion of Z_{SD} led to statistically less accurate models of TP and TSS.

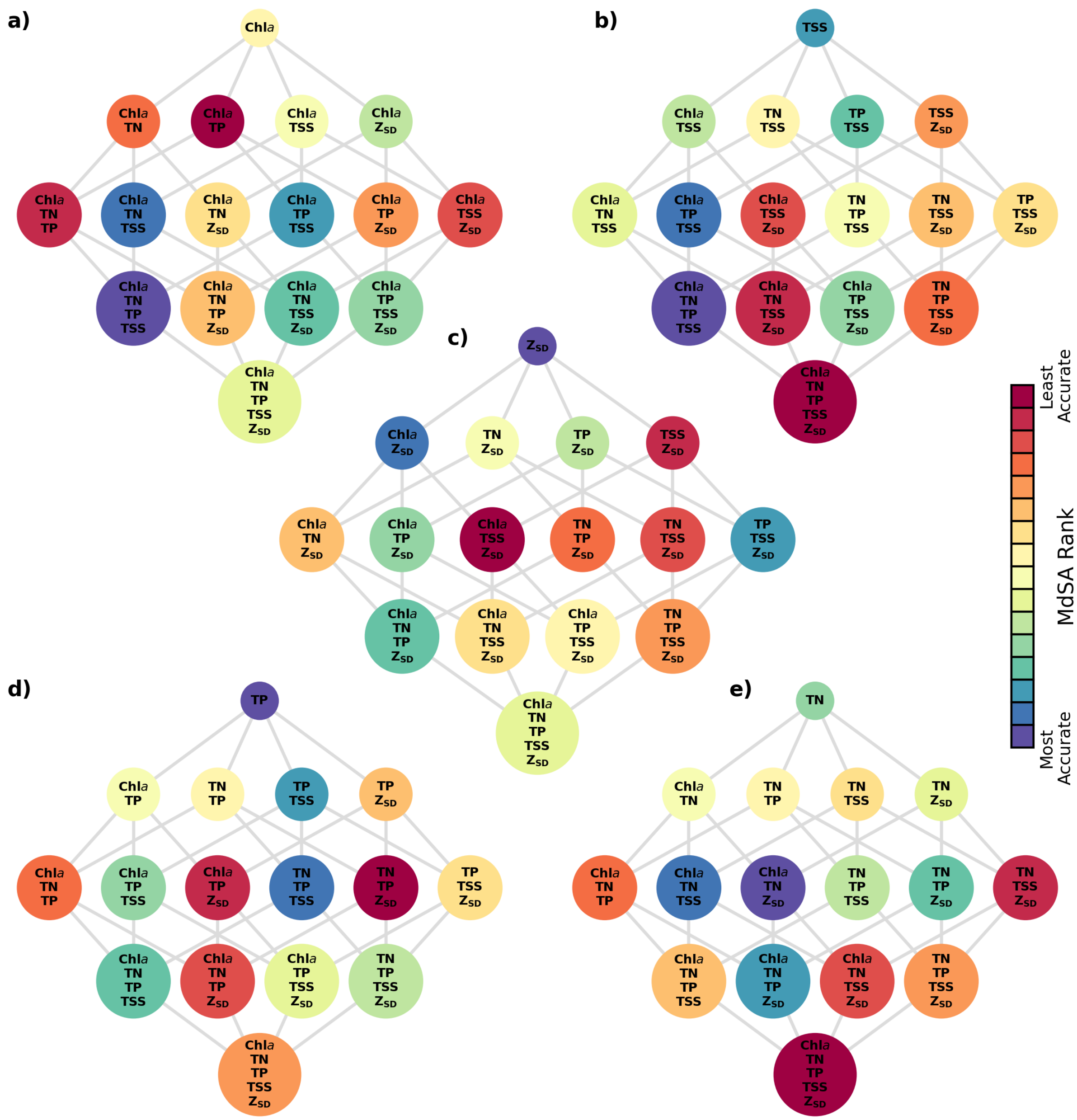

Figure 4: Performance of multiple-output MDN models for each water quality parameter (chl-*a*, TSS, Z_{SD}, TP, and TN). Each node represents a unique combination of water quality parameters used as MDN model outputs; vertical position indicates the number of outputs in that combination (1 at top to 5 at bottom). Node color indicates relative model accuracy (MdSA), ranked from most accurate (bottom of gradient bar) to least accurate (top of gradient bar) within each panel. Gray lines connect each combination to the larger combinations that contain it as a subset, illustrating how adding additional output parameters changes performance relative to the single-output model.

Feature Importance

The ranking of predictors by global importance (mean absolute SHAP value) was generally consistent across AC processors but differed slightly across WQ parameters (Supplementary Figures 1–5). SHAP analysis for the highest-ranked pipeline across all water quality parameters (RAdCor processor, ±3-days matchup window, multi-feature strategy, and single-output MDN, Figure 5) showed that Red-to-Green and Red-to-Blue ratios were the two most influential features for predicting chl-*a*, TP, TN and TSS, whereby increasing ratios (i.e., increasingly browner water) were associated with higher predicted concentrations of each WQ parameter. The direction of this influence was reversed for Z_{SD} (Figure 5d), where smaller values equate to more eutrophic conditions, and we note that $NDVI_{R/B}$ was the second most important feature for Z_{SD}. Spearman rank correlation analysis among spectral features are shown in Figure 5f. Our analysis kept both SWIR bands as a possible diagnostic of incomplete removal of the atmospheric path radiance signal. Both SWIR1 and SWIR2 bands were present and important across all AC processors including RAdCor (Figure 5), where increasing reflectance in these bands was associated with lower MDN predictions of chl-*a*, TP, TN and TSS parameters (opposite for Z_{SD}). Higher NIR reflectance was associated with higher predicted TSS concentrations, whereas higher NIR/Green ratios were associated with deeper predicted Z_{SD}.

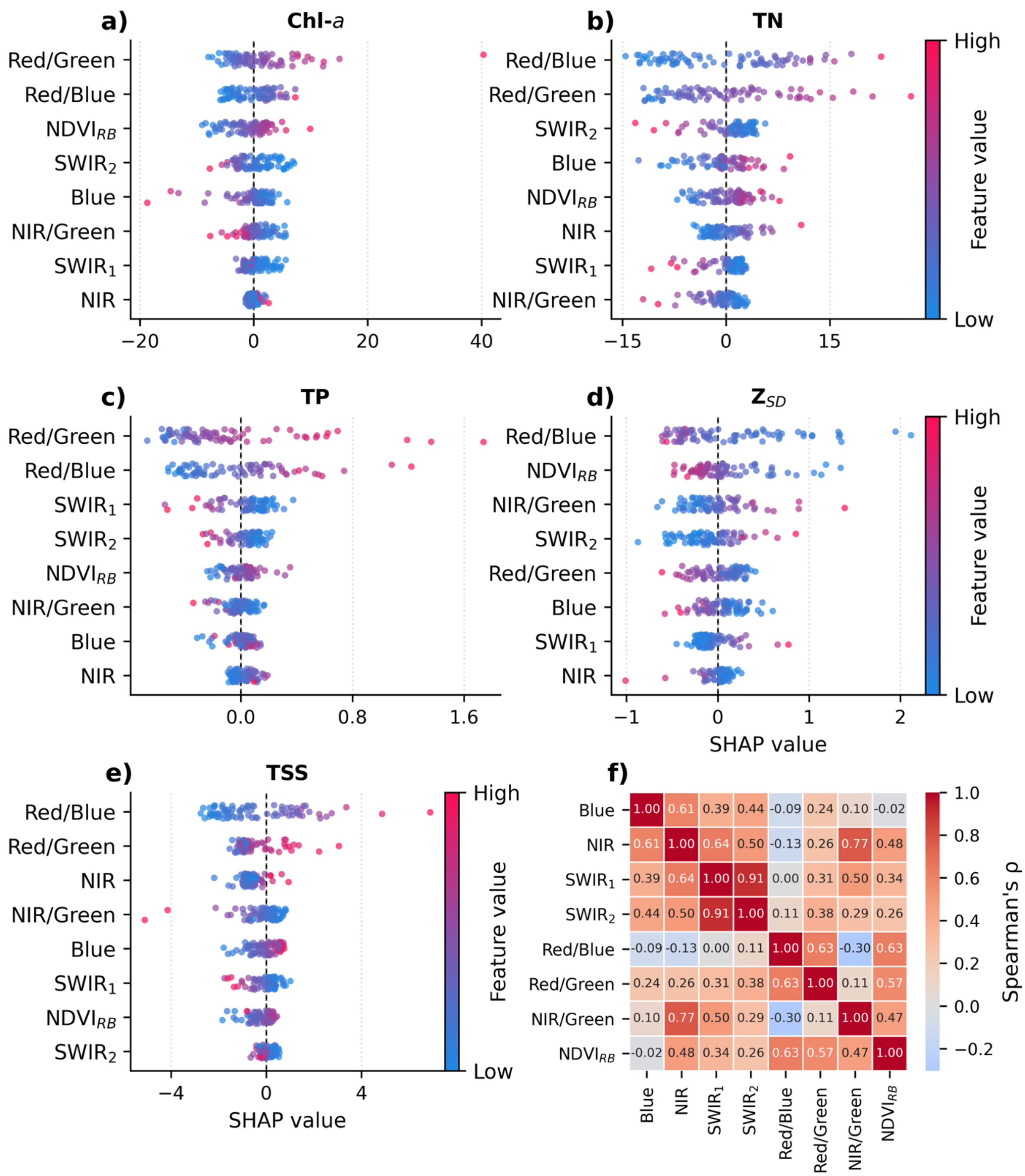

Figure 5: SHAP values for chlorophyll-a (chl-*a*), total nitrogen (TN), total phosphorus (TP), Secchi disk depth (Z_{SD}), and total suspended solids (TSS), where each dot represents an individual sample. Features are ordered from the top to bottom according to their overall importance, with those at the top having the greatest influence on model predictions. The horizontal dispersion of the dots indicates the magnitude of each feature's influence (SHAP value), while the color represents the direction of the impact of each feature on the prediction values. Panel (**f**) shows the Spearman correlation among features.

Spatial variations of nutrients

Globally, the creation of reservoirs has led to significant sediment and nutrient load reductions to many of the world's rivers (Maavara et al. 2014), and spatially explicit remote sensing data provides robust estimates of sediment trapping efficiency (Moragoda et al. 2023). The Harry S. Truman reservoir is eutrophic and has the 5th largest watershed in the state (3940 km^2; North et al., 2025). It is operated by the U.S. Army Corps of Engineers (USACE), serves as a source of drinking water, and is part of the Osage River reservoir system ultimately flowing into Lake of the Ozarks and the Missouri River. Remotely-sensed imagery of Harry S. Truman reservoir from August 19th, 2017 was used to generate spatial predictions of nutrient concentrations across the reservoir (Figure 6). To simplify the spatial analysis, we used the highest-ranked pipeline across all WQ parameters for TN and TP, consisting of the RAdCor processor, a ±3-day time window, and single-output MDN models using the multi-feature engineering strategy. There are notable spatial gradients in TN and TP concentrations across the reservoir, with the lowest nutrient concentrations at the eastern mouth of the reservoir where the dam is located. Conversely, the highest concentrations occur in the branches with the largest watersheds (South Grand River and Osage River arms), where agricultural lands dominates, while the southern and northern branches with comparatively smaller and more forested watersheds have subsequently lower TN and TP (Figure 6). *In situ* TN and TP measurements collected between 2013–2023 available through the USACE water quality monitoring program (April–September) (https://www.nwk.usace.army.mil/Locations/Water-Quality/) are generally in agreement with the spatial patterns depicted.

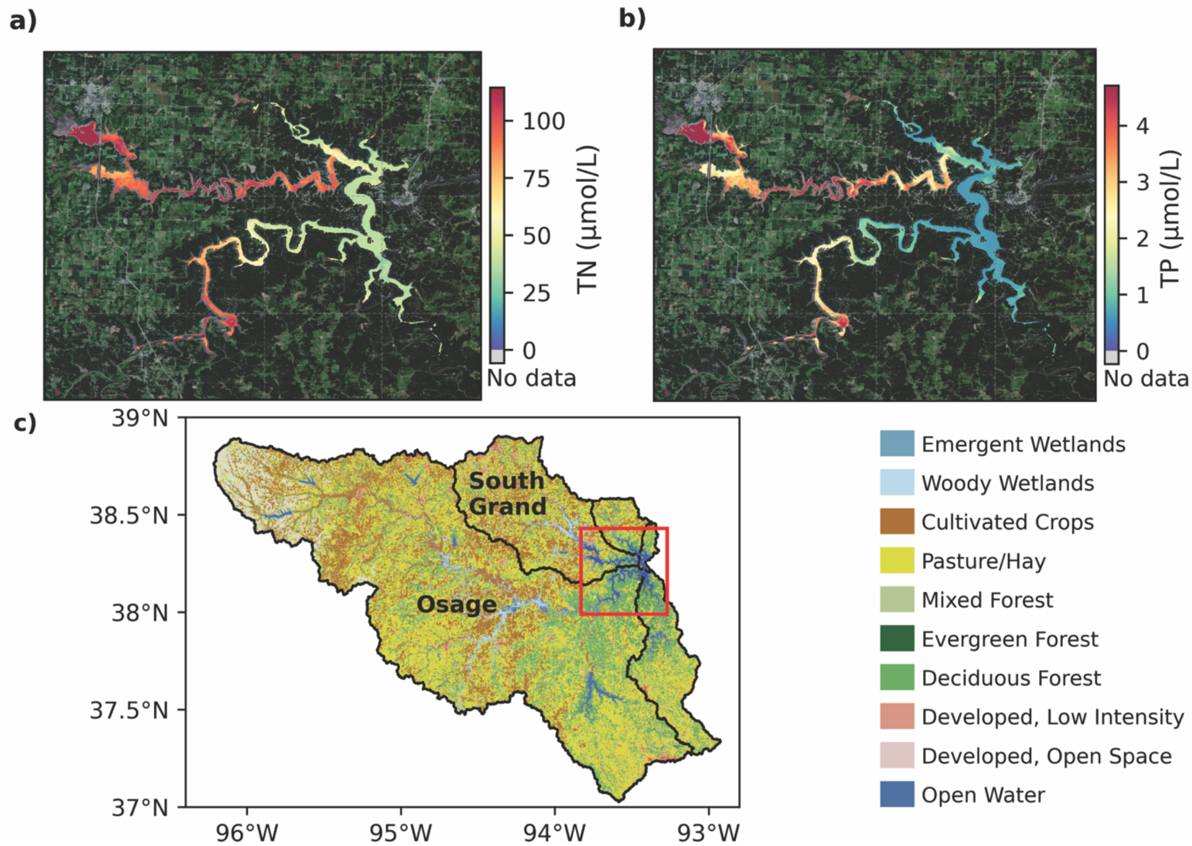

Figure 6: Water quality maps for Harry S. Truman reservoir produced using the MDN model from a near-concurrent (±3-day matchup window) Landsat 8 OLI image acquired on August 19th, 2017. **a**) total nitrogen prediction; **b**) total phosphorus prediction; **c**) watershed-scale land cover map (NLCD 2016), with the watershed boundary outlined and the reservoir extent highlighted by a red box. Landsat imagery was atmospherically corrected with RAdCor.

Discussion

Here, we demonstrate the potential of MDNs for retrieving WQ parameters beyond OACs, offering new opportunities for regional-scale assessment of nutrient pollution in optically complex waters. Our results show that MDNs, validated using *in situ* data from long-term statewide monitoring programs, can capture indirect but consistent relationships between satellite-derived R_{rs} and TN and TP, enabling regional-scale retrieval of these non-OAC. Furthermore, by combining probabilistic deep-learning with an explainable AI approach based on Shapley Additive Explanations (SHAP), we identified the most influential Landsat bands and derived ratios for nutrient retrieval, providing insight into how the model leverages indirect relationships between OACs and non-OACs. Although MDNs provide probabilistic output distributions, the present study focused on point-estimate retrieval performance. Future work could further evaluate the calibration and utility of MDN-derived predictive uncertainty for satellite-based WQ monitoring.

Our evaluation of satellite-to-field matchup windows, atmospheric correction (AC) processors, feature engineering strategies, and model output configurations further demonstrated that RAdCor processor with a ±3-day matchup window using the multi-feature engineering strategy and single-output MDN, provided the most robust overall performance across all WQ parameters. MDN retrieval performance is expected to improve when band-ratio or line-height features are included as inputs. The rationale is that band-ratio features diminish the model sensitivity to uncertainties in R_{rs} arising from AC processors (O'Shea et al., 2021; Zolfaghari et al., 2023), since ratios cancel much of the systematic bias that AC introduces across neighboring bands (Pahlevan et al., 2021a). This leaves the resulting feature's variance more strongly driven by true water-constituent signal than by residual AC noise, allowing MDN to learn a more robust relationship between reflectance and the target parameter. Indeed, our results showed that MDN models that included band combinations have on average improved accuracy and lower bias across all WQ parameters. In the future, one avenue for improving the model performance is the inclusion of ancillary data types beyond spectral reflectance; for instance, to what extent would including hydrometeorological and land cover variables as additional model inputs affect MDN performance? Intuitively, this should improve accuracy by providing catchment-scale context not captured by reflectance alone, but which variables would be most informative is yet to be explored.

Perhaps the most notable finding in this study is that chl-*a*, an optically active water constituent that directly affects water reflectance, achieved lower retrieval accuracy across every pipeline iteration compared to TN and TP that are not strictly optically active. Although TN and TP lack direct spectral signatures, they are nevertheless correlated with other OACs (Domagalski et al., 2007; Shi et al., 2017). Recent studies have demonstrated the potential of ML models for satellite-based nutrient retrieval in lakes and rivers across a range of sensors, including Sentinel-2, Sentinel-3, and MODIS, with reported MAPE values ranging from approximately 10–42% for TN and TP retrievals, depending on the study region and modeling approach (Du et al., 2018; Guo et al., 2024, 2021). While these studies differ in sensor characteristics, model architecture, and evaluation metrics, they illustrate the potential of ML models to learn how nutrient concentrations empirically co-vary with water color. Such capabilities could substantially expand the role of satellite remote sensing in environmental management and WQ monitoring by enabling routine mapping of key eutrophication drivers, rather than focusing primarily on its optical symptoms. It also should be considered the near universal difficulty in obtaining accurate chl-*a* measurements from space, both in Case-I global ocean datasets (Seegers et al., 2018) or optically complex coastal waters (Pahlevan et al., 2020). Despite being an OAC, photoacclimation, pigment-packaging and shifts in accessory pigments and cellular morphometry (Bricaud et al., 1995; Hoepffner and Sathyendranath, 1992; Sauer et al., 2012) each can serve to decouple R_{rs} from chl-*a* in complex non-linear ways that may not be readily overcome by even the most sophisticated ML models trained on comprehensive datasets. Thus the improved performance of TN and TP retrievals relative to chl-*a* from remotely-sensed data suggests that, in Missouri reservoirs, the empirical linkages between water color and nutrient concentrations is more readily retrieved than deterministic linkages between water color and chl-*a*, consistent with findings from a previous study in the same region (Pinheiro-Silva et al., 2025).

Our study reservoirs encompass a wide range of waterbody and watershed characteristics, spanning broad gradients in trophic status, land cover, and anthropogenic influence across Missouri (Jones et al., 2008a, 2008b; Pinheiro-Silva et al., 2025). Despite this substantial environmental variability in the study region, the MDN models performed well, suggesting that regionally calibrated models can successfully capture region-specific relationships between optical and biogeochemical characteristics across diverse trophic and watershed conditions. These findings also suggest that the relative importance of spectral features is likely to vary among regions, and future studies could compare SHAP patterns across different geographic areas to better understand these regional differences. Although regional recalibration is required, existing long-term monitoring programs provide a practical pathway for integrating satellite-based WQ retrievals into routine monitoring efforts by state agencies. This approach is particularly valuable as financial constraints threaten the continuity of long-term WQ monitoring programs. In this context, long-term satellite archives, such as the Landsat series, can complement field observations by providing continuous spatial coverage and helping bridge periods with limited or no *in situ* monitoring.

Differences between satellite-derived estimates and field measurements could arise from several sources, including temporal variations in WQ parameters between the satellite overpass and field sample collection. Brezonik et al. (2015) demonstrated that matchup windows of 30–60 days for lakes and a few days for large rivers can be used to match satellite images with WQ measurements and produce reliable results, depending on the temporal stability of the parameter values within a given aquatic system. In contrast, Olmanson et al. (2020) found large fluctuations in cDOM in highly colored lakes with large watersheds relative to their surface areas. Our results indicate that extending the matchup window from one to three days provides better overall performance across all WQ parameters because it increases the number of observations available for training and testing. Another source of error is the satellite AC procedure. Here, we demonstrated that depending on the AC processor, uncertainties in MDN estimates vary differently for each WQ parameter. Overall, the best model performance was obtained using RAdCor-derived estimates, followed by LEDAPS/LaSRC and ACOLITE. Although previous studies have commonly reported errors exceeding 100% when using benchmark-derived parameters, the MDNs applied to LEDAPS/LaSRC in this study achieved lower errors and, on average, outperformed ACOLITE DSF implementation. Pahlevan et al. (2021a) suggested that MDNs should be relatively insensitive to AC uncertainties in inland waters when used in association with ACOLITE. Our results partially support this recommendation, as the RAdCor implementation within ACOLITE, consistently outperformed the ACOLITE DSF and LEDAPS/LaSRC processors. This suggests that accounting for adjacency effects may provide additional benefits for MDN-based retrievals in optically complex inland waters.

Significant uncertainties and variability remain in satellite-based retrieval accuracy across diverse waterbody conditions, heavily influenced by factors such as optical complexity, atmospheric conditions, and adjacency effects. Satellite-based WQ retrieval often requires validation with *in situ* (ground-truth) measurements, yet most long-term reservoir monitoring programs are not designed to support satellite remote sensing applications mainly due to challenging logistics associated with site access, high human efforts, and financial costs (Ghosh, 2022; Llodrà-Llabrés et al., 2026). Sampling stations are commonly located near dam structures because these locations are easily accessible for routine monitoring and typically represent the deepest part of the reservoir. While this strategy is appropriate for water management, it can systematically reduce the value of monitoring data for satellite applications. Near-dam locations are often affected by shoreline mixed pixels, adjacency effects, and shadow artifacts associated with dam infrastructure, which reduce the number of high-quality satellite and *in situ* matchups available for model training and testing. In order to increase the utility of satellite remote sensing data for WQ assessment in reservoirs, we propose incorporating satellite-oriented sampling sites into long-term monitoring programs. One approach would be to retain the near-dam sampling station while establishing an additional sampling site in open-water conditions. Alternatively, when logistically feasible, the primary monitoring station could be relocated to a position that better represents open-water optical conditions. In larger or more heterogeneous reservoirs, combining near-dam stations with satellite-validation sites and additional stations along longitudinal gradients (e.g., upstream arms) would better capture spatial variability while supporting both water management and remote sensing applications. Satellite-oriented sampling sites should be selected using a criteria that maximizes the quality of satellite-*in situ* matchups. Potential considerations include maintaining a minimum distance from the shoreline, scheduling field sampling to coincide with satellite overpasses, selecting locations with sufficient water depth to minimize bottom reflectance, and collecting surface water samples. In our study, a substantial number of observations were discarded because of shoreline contamination, adjacency effects, or the absence of a satellite overpass within the selected matchup window. Incorporating these considerations into reservoir monitoring design would increase the number of usable satellite-*in situ* matchups, reduce uncertainty in satellite retrievals, improve regional models, and enhance the utility of traditional monitoring datasets for satellite remote sensing assessment.

Conclusion

In this study we presented a comprehensive evaluation of satellite-based water quality retrieval in inland waters using MDNs by evaluating key methodological choices, including atmospheric correction processors, satellite-to-field matchup windows, feature engineering strategies, and model output configurations. Using the long-term Landsat archive and *in situ* data from statewide monitoring programs in Missouri reservoirs, we demonstrated the feasibility of this framework for estimating major water quality parameters. By combining a probabilistic deep-learning framework with an explainable AI approach, such as SHAP analysis, our models effectively captured indirect relationships between R_{rs} and TN and TP, enabling retrieval of these non-optically active parameters with higher accuracy than that achieved for chl-*a*, the most extensively studied WQ parameter in remote sensing.

Acknowledgements

The authors sincerely thank the present and past students and technicians of the University of Missouri Limnology Laboratory whose efforts in collecting, processing, and analyzing the long-term water quality data made this study possible.

Funding

This work was supported by the NASA Remote Sensing of Water Quality program award number 80NSSC22K0771. The data is based on work supported by the Missouri Department of Natural Resources (MDNR), which funds the Missouri Statewide Lake Assessment Program (SLAP), coordinated by the University of Missouri Limnology Laboratory. Part of the data was also obtained through the Lakes of Missouri Volunteer Program (LMVP) funded by MDNR. Although the information described here has been funded wholly or in part by the United States Environmental Protection Agency and the Missouri Department of Natural Resources under four assistance Agreements to the Curators of the University of Missouri, it has not been subjected to the Agency's product and administrative review and therefore might not necessarily reflect the views of these agencies; no official endorsement should be inferred.

References

Bishop, C.M., 1994. Mixture Density Networks.

Brezonik, P.L., Olmanson, L.G., Finlay, J.C., Bauer, M.E., 2015. Factors affecting the measurement of CDOM by remote sensing of optically complex inland waters. Remote Sens. Environ. 157, 199–215.

Bricaud, A., Babin, M., Morel, A., Claustre, H., 1995. Variability in the chlorophyll-specific absorption coefficients of natural phytoplankton: Analysis and parameterization. J. Geophys. Res. Oceans 100, 13,321–13,332.

Castagna, A., Vanhellemont, Q., 2025. A generalized physics-based correction for adjacency effects. Appl. Opt. 64, 2719.

Chebud, Y., Naja, G.M., Rivero, R.G., Melesse, A.M., 2012. Water quality monitoring using remote sensing and an artificial neural network. Water Air Soil Pollut. 223, 4875–4887.

Conley, D.J., Paerl, H.W., Howarth, R.W., Boesch, D.F., Seitzinger, S.P., Havens, K.E., Lancelot, C., Likens, G.E., 2009. Ecology - Controlling eutrophication: Nitrogen and phosphorus. Science (1979).

Domagalski, J., Lin, C., Luo, Y., Kang, J., Wang, S., Brown, L.R., Munn, M.D., 2007. Eutrophication study at the Panjiakou-Daheiting Reservoir system, northern Hebei Province, People’s Republic of China: Chlorophyll-a model and sources of phosphorus and nitrogen. Agric. Water Manag. 94, 43–53.

Dong, G., Hu, Z., Liu, X., Fu, Y., Zhang, W., 2020. Spatio-temporal variation of total nitrogen and ammonia nitrogen in the water source of the middle route of the south-to-north water diversion project. Water (Switzerland) 12.

Du, C., Wang, Q., Li, Y., Lyu, H., Zhu, L., Zheng, Z., Wen, S., Liu, G., Guo, Y., 2018. Estimation of total phosphorus concentration using a water classification method in inland water. International Journal of Applied Earth Observation and Geoinformation 71, 29–42.

Ghosh, A., 2022. Does Our Idea of Diversity, Equity, Inclusion, and Justice (DIEJ) Impact Our Research Output? Limnol. Oceanogr. Bull. 31, 69–71.

Guo, H., Huang, J.J., Chen, B., Guo, X., Singh, V.P., 2021. A machine learning-based strategy for estimating non-optically active water quality parameters using Sentinel-2 imagery. Int. J. Remote Sens. 42, 1841–1866.

Guo, H., Huang, J.J., Zhu, X., Tian, S., Wang, B., 2024. Spatiotemporal variation reconstruction of total phosphorus in the Great Lakes since 2002 using remote sensing and deep neural network. Water Res. 255, 121493.

Guo, H., Tian, S., Jeanne Huang, J., Zhu, X., Wang, B., Zhang, Z., 2022. Performance of deep learning in mapping water quality of Lake Simcoe with long-term Landsat archive. ISPRS Journal of Photogrammetry and Remote Sensing 183, 451–469.

Hoepffner, N., Sathyendranath, S., 1992. Bio-optical characteristics of coastal waters: Absorption spectra of phytoplankton and pigment distribution in the western North Atlantic. Limnol. Oceanogr. 37, 1660–1679.

Jones, J.R., Argerich, A., Obrecht, D. V, Thorpe, A.P., North, R.L., 2024a. Missouri Lakes and Reservoirs Long-term Limnological Dataset, 1976-2018. Environmental Data Initiative 2.

Jones, J.R., Knowlton, M.F., Obrecht, D. V., 2008a. Role of land cover and hydrology in determining nutrients in mid-continent reservoirs: Implications for nutrient criteria and management. Lake Reserv. Manag. 24, 1–9.

Jones, J.R., North, R.L., Argerich, A., Thorpe, A.P., Obrecht, D. V, Price, A., Santamaria, K., Richardson, D.C., 2024b. Missouri reservoir profile data including temperature, depth, and oxygen profiles (1989-2022). Environmental Data Initiative 2.

Jones, J.R., Obrecht, D. V., Perkins, B.D., Knowlton, M.F., Thorpe, A.P., Watanabe, S., Bacon, R.R., 2008b. Nutrients, seston, and transparency of Missouri reservoirs and oxbow lakes: An analysis of regional limnology. Lake Reserv. Manag. 24, 155–180.

Li, Y., Zhang, Yunlin, Shi, K., Zhu, G., Zhou, Y., Zhang, Yibo, Guo, Y., 2017. Monitoring spatiotemporal variations in nutrients in a large drinking water reservoir and their relationships with hydrological and meteorological conditions based on Landsat 8 imagery. Science of the Total Environment 599–600, 1705–1717.

Lin, S., Qi, J., Jones, J.R., Stevenson, R.J., 2018. Effects of sediments and coloured dissolved organic matter on remote sensing of chlorophyll-a using Landsat TM/ETM+ over turbid waters. Int. J. Remote Sens. 39, 1421–1440.

Llodrà-Llabrés, J., Pérez-Girón, J.C., Postma, T., Pérez-Martínez, C., Alcaraz-Segura, D., Martínez-López, J., 2026. Satellite Solutions: Facing Chlorophyll-a Retrieval in Small Mountain Lakes in the Sierra Nevada, Spain. Water Resour. Res. 62, e2026WR043523.

Maciel, F.P., Pedocchi, F., 2022. Evaluation of ACOLITE atmospheric correction methods for Landsat-8 and Sentinel-2 in the Río de la Plata turbid coastal waters. Int. J. Remote Sens. 43, 215–240.

Maavara, T., Dürr, H.H., Van Cappellen, P., 2014. Worldwide retention of nutrient silicon by river damming: From sparse data set to global estimate. Global Biogeochem. Cycles 28, 842–855.

Meyer, M.F., Topp, S.N., King, T. V., Ladwig, R., Pilla, R.M., Dugan, H.A., Eggleston, J.R., Hampton, S.E., Leech, D.M., Oleksy, I.A., Ross, J.C., Ross, M.R.V., Woolway, R.I., Yang, X., Brousil, M.R., Fickas, K.C., Padowski, J.C., Pollard, A.I., Ren, J., Zwart, J.A., 2024. National-scale remotely sensed lake trophic state from 1984 through 2020. Sci. Data 11, 77.

Moragoda, N., Cohen, S., Gardner, J., Muñoz, D., Narayanan, A., Moftakhari, H., Pavelsky, T. M., 2023. Modeling and analysis of sediment trapping efficiency of large dams using remote sensing. Water Resour. Res. 59, e2022WR033296.

Morley, S.K., Brito, T. V., Welling, D.T., 2018. Measures of Model Performance Based On the Log Accuracy Ratio. Space Weather 16, 69–88.

North, R.L., Argerich, A., Obrecht, D. V, Thorpe, A.P., Richardson, D.C., 2025. Missouri reservoir water quality data from the Statewide Lake Assessment Program (SLAP), the Lakes of Missouri Volunteer Program (LMVP), and the Reservoir Observer Student Scientists (ROSS) program. Environmental Data Initiative.

North, R.L., Richardson, D.C., Price, A., Pinheiro-Silva, L., Silsbe, G.M., 2025. Missouri reservoir water quality data (2022 - current) from the Statewide Lake Assessment Program (SLAP) ver 2. Environmental Data Initiative.

Ogashawara, I., Wollrab, S., Berger, S.A., Kiel, C., Jechow, A., Guislain, A.L.N., Gege, P., Ruhtz, T., Hieronymi, M., Schneider, T., Lischeid, G., Singer, G.A., Hölker, F., Grossart, H.P., Nejstgaard, J.C., 2024. Unleashing the power of remote sensing data in aquatic research: Guidelines for optimal utilization. Limnol. Oceanogr. Lett. 9, 667–673.

Olmanson, L.G., Page, B.P., Finlay, J.C., Brezonik, P.L., Bauer, M.E., Griffin, C.G., Hozalski, R.M., 2020. Regional measurements and spatial/temporal analysis of CDOM in 10,000+ optically variable Minnesota lakes using Landsat 8 imagery. Science of the Total Environment 724, 138141.

O'Shea, R.E., Pahlevan, N., Smith, B., Bresciani, M., Egerton, T., Giardino, C., Li, L., Moore, T., Ruiz-Verdu, A., Ruberg, S., Simis, S.G.H., Stumpf, R., Vaičiūtė, D., 2021. Advancing cyanobacteria biomass estimation from hyperspectral observations: Demonstrations with HICO and PRISMA imagery. Remote Sens. Environ. 266, 112693.
Pahlevan, N., Mangin, A., Balasubramanian, S. V., Smith, B., Alikas, K., Arai, K., Barbosa, C., Bélanger, S., Binding, C., Bresciani, M., Giardino, C., Gurlin, D., Fan, Y., Harmel, T., Hunter, P., Ishikaza, J., Kratzer, S., Lehmann, M.K., Ligi, M., Ma, R., Martin-Lauzer, F.R., Olmanson, L., Oppelt, N., Pan, Y., Peters, S., Reynaud, N., Sander de Carvalho, L.A., Simis, S., Spyrakos, E., Steinmetz, F., Stelzer, K., Sterckx, S., Tormos, T., Tyler, A., Vanhellemont, Q., Warren, M., 2021a. ACIX-Aqua: A global assessment of atmospheric correction methods for Landsat-8 and Sentinel-2 over lakes, rivers, and coastal waters. Remote Sens. Environ. 258, 112366.
Pahlevan, N., Smith, B., Alikas, K., Anstee, J., Barbosa, C., Binding, C., Bresciani, M., Cremella, B., Giardino, C., Gurlin, D., Fernandez, V., Jamet, C., Kangro, K., Lehmann, M.K., Loisel, H., Matsushita, B., Hà, N., Olmanson, L., Potvin, G., Simis, S.G.H., VanderWoude, A., Vantrepotte, V., Ruiz-Verdù, A., 2022. Simultaneous retrieval of selected optical water quality indicators from Landsat-8, Sentinel-2, and Sentinel-3. Remote Sens. Environ. 270, 112860.
Pahlevan, N., Smith, B., Binding, C., Gurlin, D., Li, L., Bresciani, M., Giardino, C., 2021b. Hyperspectral retrievals of phytoplankton absorption and chlorophyll-a in inland and nearshore coastal waters. Remote Sens. Environ. 253, 112200.
Pahlevan, N., Smith, B., Schalles, J., Binding, C., Cao, Z., Ma, R., Alikas, K., Kangro, K., Gurlin, D., Hà, N., Matsushita, B., Moses, W., Greb, S., Lehmann, M.K., Ondrusek, M., Oppelt, N., Stumpf, R., 2020. Seamless retrievals of chlorophyll-a from Sentinel-2 (MSI) and Sentinel-3 (OLCI) in inland and coastal waters: A machine-learning approach. Remote Sens. Environ. 240, 111604.
Pinheiro-Silva, L., Silsbe, G.M., Richardson, D.C., North, R.L., 2025. Long-term trends and drivers of water color in Missouri reservoirs. Front. Environ. Sci. 13, 1725096.
Renosh, P.R., Doxaran, D., De Keukelaere, L., Gossn, J.I., 2020. Evaluation of atmospheric correction algorithms for sentinel-2-MSI and sentinel-3-OLCI in highly turbid estuarine waters. Remote Sens. 12, 1285.
Saranathan, A.M., Werther, M., Balasubramanian, S.V., Odermatt, D., Pahlevan, N., 2024. Assessment of advanced neural networks for the dual estimation of water quality indicators and their uncertainties. Front. Remote Sens. 5, 1383147.
Sauer, M.J., Roesler, C.S., Werdell, P.J., Barnard, A., 2012. Under the hood of satellite empirical chlorophyll a algorithms: revealing the dependencies of maximum band ratio algorithms on inherent optical properties. Opt. Express 20, 20920–20933.
Seegers, B.N., Stumpf, R.P., Schaeffer, B.A., Loftin, K.A., Werdell, P.J., 2018. Performance metrics for the assessment of satellite data products: an ocean color case study. Opt. Express 26, 7404.
Shapley, L.S., 1953. A value for n-person games. In: Kuhn, H.W., Tucker, A.W. (Eds.), Contributions to the Theory of Games, Volume II. Princeton University Press, Princeton, NJ, pp. 307–317.
Shi, K., Zhang, Y., Zhou, Y., Liu, X., Zhu, G., Qin, B., Gao, G., 2017. Long-Term MODIS observations of cyanobacterial dynamics in Lake Taihu: Responses to nutrient enrichment and meteorological factors. Sci. Rep. 7, 40326.

Smith, B., Pahlevan, N., Schalles, J., Ruberg, S., Errera, R., Ma, R., Giardino, C., Bresciani, M., Barbosa, C., Moore, T., Fernandez, V., Alikas, K., Kangro, K., 2021. A Chlorophyll-a Algorithm for Landsat-8 Based on Mixture Density Networks. Front. Remote Sens. 1, 623678.
Smith, V.H., Schindler, D.W., 2009. Eutrophication science: where do we go from here? Trends Ecol. Evol. 24, 201–207.
Sun, D., Qiu, Z., Li, Y., Shi, K., Gong, S., 2014. Detection of total phosphorus concentrations of turbid inland waters using a remote sensing method. Water Air Soil Pollut. 225, 1953.
Vanhellemont, Q., 2019. Adaptation of the dark spectrum fitting atmospheric correction for aquatic applications of the Landsat and Sentinel-2 archives. Remote Sens. Environ. 225, 175–192.
Vanhellemont, Q., Ruddick, K., 2018. Atmospheric correction of metre-scale optical satellite data for inland and coastal water applications. Remote Sens. Environ. 216, 586–597.
Wang, D., Ma, R., Xue, K., Loiselle, S.A., 2019. The assessment of landsat-8 OLI atmospheric correction algorithms for inland waters. Remote Sens. 11, 169.
Wu, C., Wu, J., Qi, J., Zhang, L., Huang, H., Lou, L., Chen, Y., 2010. Empirical estimation of total phosphorus concentration in the mainstream of the Qiantang River in China using Landsat TM data. Int. J. Remote Sens. 31, 2309–2324.
Xiong, J., Lin, C., Cao, Z., Hu, M., Xue, K., Chen, X., Ma, R., 2022. Development of remote sensing algorithm for total phosphorus concentration in eutrophic lakes: Conventional or machine learning? Water Res. 215, 118213.
Zhu, L., Cui, T., Runa, A., Pan, X., Zhao, W., Xiang, J., Cao, M., 2024. Robust remote sensing retrieval of key eutrophication indicators in coastal waters based on explainable machine learning. ISPRS J. Photogramm. Remote Sens. 211, 262–280.
Zhu, X., Guo, H., Huang, J.J., Tian, S., Xu, W., Mai, Y., 2022. An ensemble machine learning model for water quality estimation in coastal area based on remote sensing imagery. J. Environ. Manage. 323, 116187.
Zolfaghari, K., Pahlevan, N., Simis, S.G.H., O'Shea, R.E., Duguay, C.R., 2023. Sensitivity of remotely sensed pigment concentration via Mixture Density Networks (MDNs) to uncertainties from atmospheric correction. J. Great Lakes Res. 49, 341–356.